Zhou *et al.*
European Journal of Medical Research (2025) 30:214
https://doi.org/10.1186/s40001-025-02471-0

European Journal of Medical Research

RESEARCH

Open Access

Integrative analysis of bulk and single-cell sequencing reveals TNFSF9 as a potential regulator in microsatellite instability stomach adenocarcinoma

Jianlong Zhou[1†], Yucheng Zhang[1†], Yongfeng Liu[1†], Jiehui Li[1], Wenxing Zhang[1], Junjiang Wang[1], Xueqing Yao[1,3], Huolun Feng[1,2*], Jiabin Zheng[1*] and Yong Li[1,2*]

Abstract

Background Stomach adenocarcinoma (STAD) with microsatellite instability (MSI) is associated with a better prognosis compared to Non-MSI. This study aims to elucidate the differences in the tumor microenvironment (TME) of MSI and explore its underlying mechanisms in STAD.

Methods TME differences between MSI and Non-MSI were analyzed using single-cell RNA sequencing (MSI = 7, Non-MSI = 19) and bulk RNA sequencing (MSI = 39, Non-MSI = 198). Differentially expressed genes (DEGs) were used to identify enriched pathways and hub genes. TNFSF9 expression was validated by immunohistochemistry (IHC) on 23 STAD sections (MSI = 13, Non-MSI = 10) and confirmed in tumor epithelial cells using SNU-1 (MSI) and AGS (Non-MSI) cell lines through quantitative polymerase chain reaction (qPCR) and Western blot (WB).

Results The results showed MSI was significantly associated with a better prognosis ($P < 0.05$). Within the TME, MSI was associated with a higher abundance of antigen-presenting cells, including M1 macrophages (40.1% vs. 27.9%) and activated dendritic cells (22.1% vs. 10.5%), as well as pro-inflammatory Th1-like $CD4^+$ T cells (15% vs. 11%). However, MSI also showed an increase in exhausted T cells, indicating a complex immune landscape. Signaling pathway and cell communication analyses revealed an enrichment of cytokine-related pathways in MSI. Hub gene analysis revealed that TNFSF9 was predominantly expressed in stromal cells and partially in tumor epithelial cells in MSI, with its upregulation further confirmed through IHC, qPCR, and WB. Correlation analysis demonstrated a positive relationship between TNFSF9 expression and the abundance of M1 macrophages.

Conclusions These findings provide new insights into the TME of MSI in STAD, emphasizing the significant role of TNFSF9 in shaping MSI-specific TME, enhancing immunotherapy efficacy, and improving patient survival.

Keywords Microsatellite instability, Stomach adenocarcinoma, TME, TNFSF9, Prognosis

†Jianlong Zhou, Yucheng Zhang and Yongfeng Liu have contributed equally to this work.

*Correspondence:
Huolun Feng
fenghuolun2022@qq.com
Jiabin Zheng
zhengjiabin@gdph.org.cn
Yong Li
liyong@gdph.org.cn
Full list of author information is available at the end of the article

Introduction

Stomach adenocarcinoma (STAD) is classified into four subtypes based on molecular phenotypes in The Cancer Genome Atlas (TCGA): MSI (microsatellite instability tumors), EBV (Epstein–Barr virus-positive tumors), GS (genomically stable tumors), and CIN (chromosomal instability tumors) [1]. Among these subtypes, MSI is associated with a more favorable prognosis. MSI is characterized by the loss of DNA mismatch repair function and is primarily detected via immunohistochemistry or polymerase chain reaction [2, 3]. Clinical trials demonstrate that STAD with MSI shows better outcomes when treated with immune checkpoint inhibitors like PD-1 or PD-L1 inhibitors [4–6]. Moreover, recent studies indicate that MSI, irrespective of adjuvant therapy, is linked to a favorable prognosis in STAD [7–9]. In summary, MSI is strongly linked to better survival and prognosis.

MSI, characterized by a higher frequency of gene mutations and an increased proportion of neoantigen peptides, promotes a highly immunogenic environment in STAD [10]. MSI enhances the tumor immune response, evidenced by abundant $CD8^+$ T-cell infiltration [11, 12]. Previous studies analyzed differences in the tumor microenvironment (TME) using bulk RNA sequencing (bulk RNA-seq), which is limited in capturing interactions among diverse cell types. Furthermore, these studies did not explore the molecular mechanisms underlying immune infiltration differences [13]. Recently, single-cell RNA sequencing (scRNA-seq) has demonstrated advantages in describing tumor complexity and heterogeneity [14–18]. Integration of bulk RNA-seq and scRNA-seq enables a systematic exploration of differences in molecular mechanisms and prognosis between MSI and Non-MSI.

Our study aims to unravel the differences in the TME and underlying mechanisms between MSI and Non-MSI. These findings could improve clinical diagnosis and suggest new therapeutic strategies for STAD.

Materials and methods

Data collection

Cohorts were classified into MSI (MSI-H) and Non-MSI (MSS and MSI-L). Immunohistochemistry (IHC) was conducted on samples classified as MSI (deficient mismatch repair) and Non-MSI (proficient mismatch repair). The scRNA-seq data were sourced from the GSE183904 dataset, which includes 48 samples, with 26 tumor samples analyzed for this study. Bulk RNA-seq data were acquired from the GSE62254 dataset. Additionally, the TCGA database was used to assess TNFSF9 expression differences between MSI and Non-MSI. The study sourced 23 STAD pathological sections from the Guangdong Provincial People's Hospital in China, categorized into two groups based on their postoperative pathological IHC results: 13 samples were identified as MSI, while the remaining 10 were recognized as Non-MSI.

The study was conducted with the necessary ethical approval obtained from the Institutional Review Board. Informed written consent was obtained from all participating patients, ensuring their voluntary participation and understanding of the study's objectives and procedures.

Estimation of immune cell infiltration in bulk RNA-seq

The "CIBERSORT" algorithm [19] was applied to calculate the proportion of 22 immune infiltrating cells for each sample based on the LM22 signature for 100 permutations. The differences in immune cell subtypes between the MSI and Non-MSI from the bulk RNA-seq data (GSE62254) were analyzed.

Estimation of immune cell infiltration in scRNA-seq

ScRNA-seq data were transformed into Seurat objects using the "CreateSeuratObject" algorithm in the "Seurat" package with R software (version 4.1.2) [20]. Data quality control was performed with the following criteria: UMI count < 6000, gene count ≥ 250, and mitochondrial gene ratio < 0.20. We used R package "Harmony" to remove batch effects between different patients [21]. Non-linear dimensional reduction was performed using the UMAP method. Cell clustering was performed using the "FindClusters" function in Seurat, and the clusters were annotated by the expression of canonical marker genes [16–18]. The R package "CellChat" is a tool used to infer, analyze and visualize intercellular communication networks [22]. "CellChat" quantitatively characterizes and compares intercellular communications by analyzing signaling inputs and outputs for cell populations based on the known structural composition of ligand–receptor interactions.

Differentially expressed genes (DEGs) and pathway analysis

The R package "Limma" was used for DEGs analysis. An empirical Bayesian method estimated the fold change between clusters one and two, identified via consensus clustering, using moderated T-tests [23]. Adjusted P-values for multiple testing were calculated using the Benjamini–Hochberg correction. Genes with an absolute log2 fold change greater than 0.25 were identified as DEGs between MSI and Non-MSI. Pathway and functional enrichment analyses, including Gene Set Enrichment Analysis (GSEA), the Kyoto Encyclopedia of Genes and Genomes (KEGG), and Gene Ontology (GO), were performed using the R packages "ClusterProfiler" (version

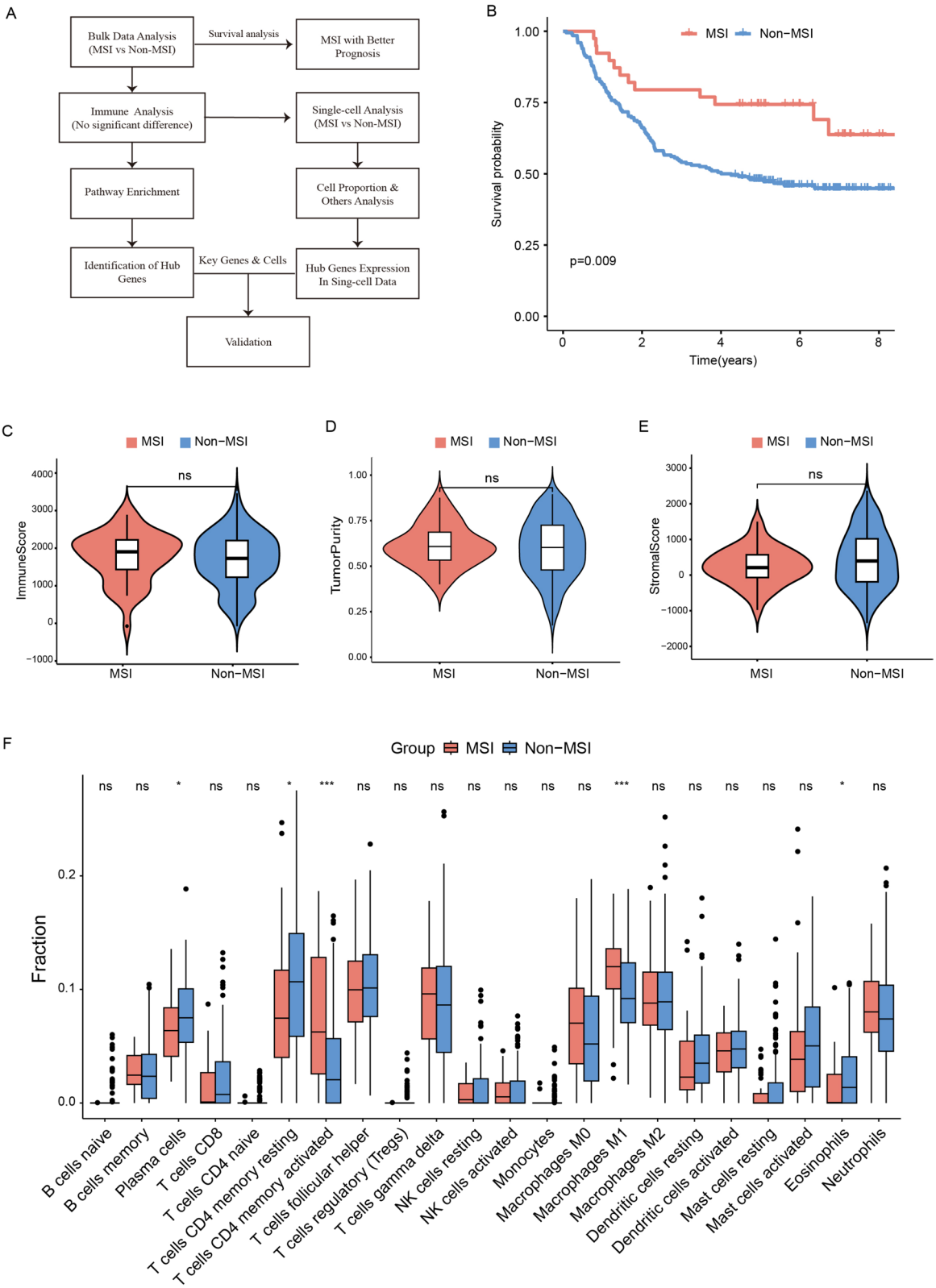

Fig. 1 Inter-tumor TME heterogeneity between MSI and Non-MSI in bulk RNA-seq analysis. **A** Experimental design overview. **B** Kaplan–Meier survival curves for STAD comparing MSI and Non-MSI. **C**–**E** Comparisons of ImmuneScore, TumorPurity, and StromalScore between MSI and Non-MSI. **F** Boxplots illustrating the proportions of 22 immune infiltrating cells between MSI and Non-MSI. *$P < 0.05$; **$P < 0.01$; ***$P < 0.001$; ****$P < 0.0001$; ns: not significant

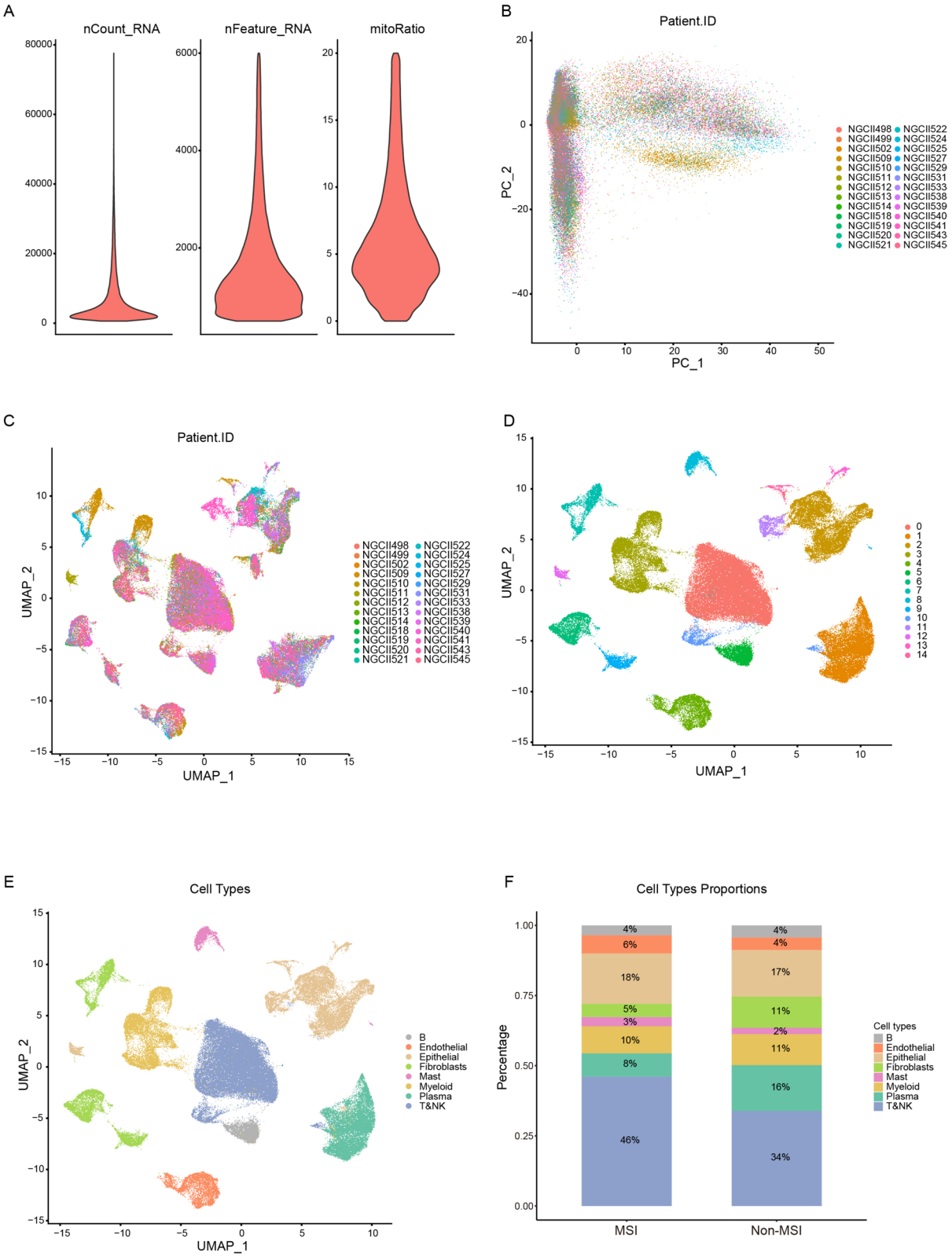

Fig. 2 The single-cell landscape of STAD. **A** Violin plots of RNA counts (nCount_RNA), RNA features (nFeature_RNA), and Mitochondrial RNA ratio (mitoRatio) after data filtering. **B** DimPlot showing patient-specific clustering via PCA for single-cell data. **C** UMAP plot visualizing patient.IDs in STAD after correcting for batch effects. **D** UMAP plot illustrating the clustering of STAD cells. **E** UMAP plot revealing cell lineages marked by specific genes in STAD. **F** Histograms illustrating the proportions of STAD cells between MSI and Non-MSI

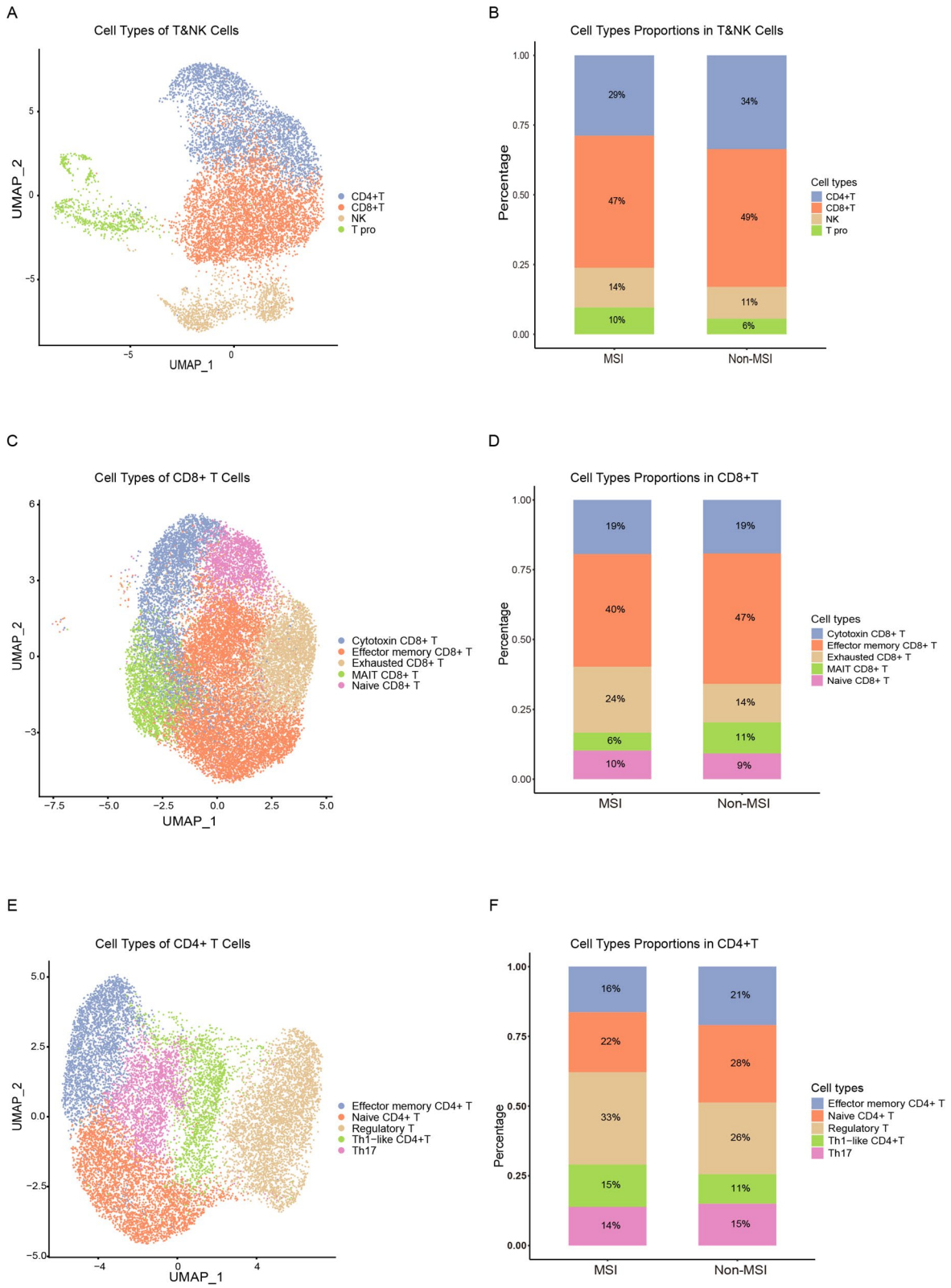

Fig. 3 A single-cell atlas of lymphocytes. **A** UMAP plot displaying cell lineages identified by specific marker genes in T&NK cells. **B** Histograms showing the proportions of T&NK cells between MSI and Non-MSI. **C** UMAP plot displaying cell lineages identified by specific marker genes in $CD8^+$ T cells. **D** Histograms showing the proportions of $CD8^+$ T cells between MSI and Non-MSI. **E** UMAP plot displaying cell lineages identified by specific marker genes in $CD4^+$ T cells. **F** Histograms showing the proportions of $CD4^+$ T cells between MSI and Non-MSI

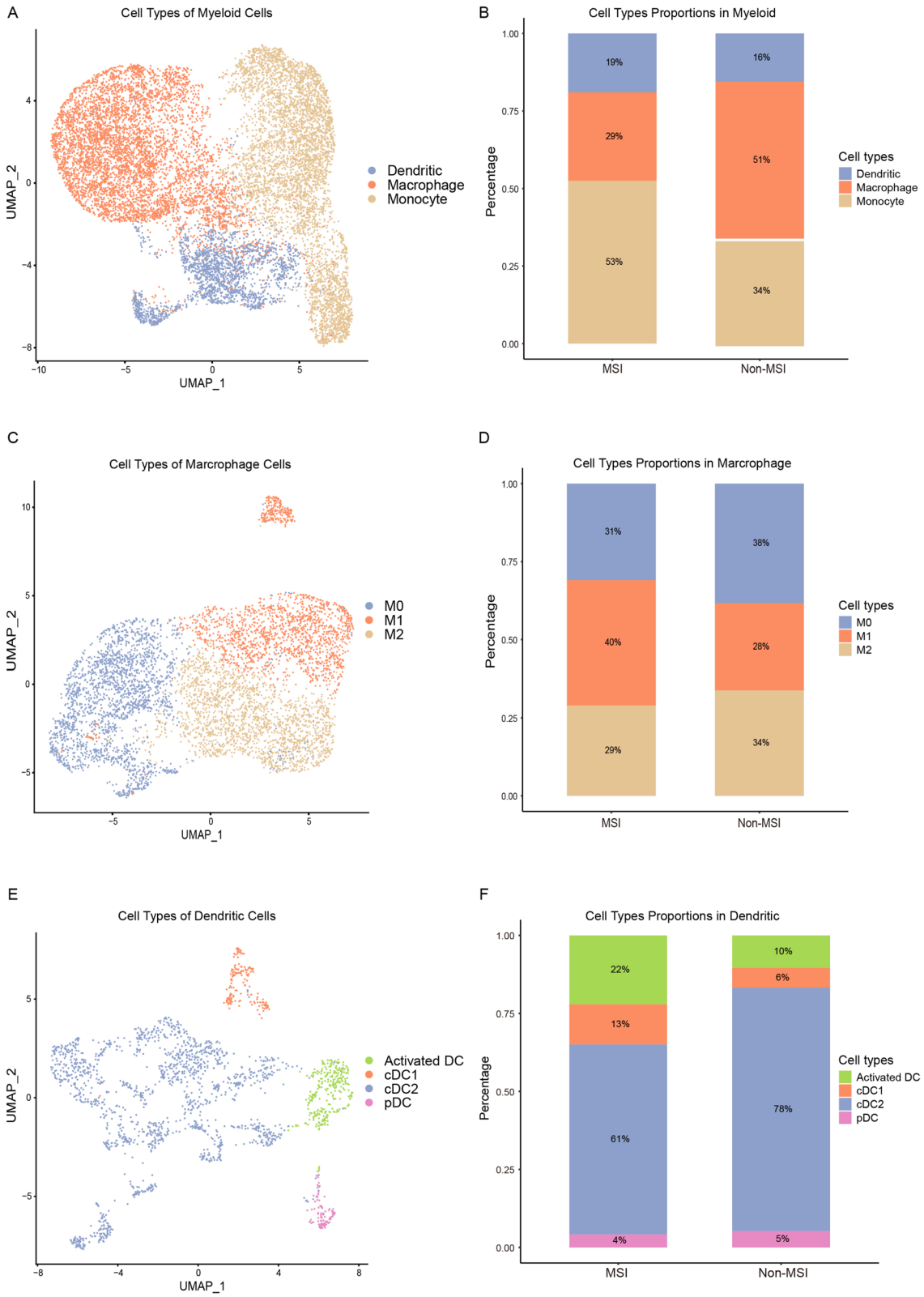

Fig. 4 A single-cell atlas of myeloid cells. **A** UMAP plot displaying cell lineages identified by specific marker genes in myeloid cells. **B** Histograms showing the proportions of myeloid cells between MSI and Non-MSI. **C** UMAP plot displaying cell lineages identified by specific marker genes in macrophages. **D** Histograms showing the proportions of macrophages between MSI and Non-MSI. **E** UMAP plot displaying cell lineages identified by specific marker genes in dendritic cells. **F** Histograms showing the proportions of dendritic cells between MSI and Non-MSI

4.0.5), "org.Hs.eg.db" (version 3.13.0), "ggplot2" (version 3.3.5), and "enrichplot" (version 1.12.3) [24].

Definition and validation of hub genes

Hub genes were identified as the intersection of cytokine-related pathways derived from GSEA, KEGG, and GO enrichment analyses, resulting in 8 hub genes. Their expression patterns were then verified at both the bulk RNA-seq and scRNA-seq levels. Notably, among these hub genes, TNFSF9 showed higher expression in both bulk RNA-seq and scRNA-seq. Finally, the significance of TNFSF9 was validated using public database analyses and experimental data.

IHC

For IHC analysis, paraffin-embedded tissue sections were incubated with TNFSF9 antibody overnight at 4 °C, treated with secondary antibodies, and visualized using the DAB staining protocol, followed by hematoxylin counterstaining for background clarity. The assessment of the area and density of stained regions, as well as the integrated optical density (IOD) of the IHC sections, was performed using Image-Pro Plus software version 6.0 (Media Cybernetics, Rockville, MD, USA, https://mediacy.com/). The evaluation of density signals within five randomly selected fields of the tissue sections was carried out in a blinded manner, followed by a statistical analysis to determine their significance.

Cell culture and quantitative polymerase chain reaction (qPCR)

The SNU-1 cell line, classified as MSI, and the AGS cell line, classified as Non-MSI [25], were cultured in 1640 medium supplemented with 10% fetal bovine serum under conditions of 5% CO2, 37 °C, and humidified environment. A total of 1×10^6 cells from each type were selected for subsequent qPCR analysis. Total RNA extraction from the cells was performed using Tissue RNA Purification Kit Plus (EZBioscience, cat# EZB-RN001-plus). 1 μg RNA was used for reverse transcription using the Colour Reverse Transcriptase Kit (EZBioscience, cat# A0010CGQ). Gene expression was quantified by qPCR using SYBR Green qPCR Mix (EZBioscience, cat# A0012-R2). For qPCR analysis, specific primers for TNFSF9 were used, with the forward primer sequence as 5′-AAATGTTCTGATCGATGGG-3′ and the reverse primer sequence 5′-CCGCAGCTCTAG TTGAAAGAAGA-3′ [26]. The expression levels were normalized to GAPDH, and the qPCR reaction was performed using a CFX96 Real-Time PCR Detection System (Bio-Rad). The relative expression of TNFSF9 was calculated using the $2^{-\Delta\Delta Ct}$ method.

Western blot analysis

Cells were lysed using M-PER Mammalian Protein Extraction Reagent (Thermo Scientific), followed by sodium dodecyl sulfate–polyacrylamide gel electrophoresis. The membrane was blocked with 5% non-fat dry milk in TBST for 1 h at room temperature. After blocking, the membrane was incubated overnight at 4 °C with a TNFSF9 monoclonal antibody (Proteintech, cat# 66450-1-lg). The following day, the membrane was washed with TBST and incubated with a secondary antibody for 1 h at room temperature. After additional washing, the membranes were visualized using the Tanon 4600 chemiluminescence imaging system (Tanon, Shanghai, China), with Immobilon Western Chemiluminescent HRP Substrate (Millipore). Quantification of a specific protein was achieved by calculating the ratio of its intensity bands to those of α-Tubulin, utilizing the ImageJ software for analysis.

Survival analysis

Statistical analyses were performed using R software (version 4.1.2). Gene expression data were log2 transformed and standardized. The Wilcoxon test was used to compare TNFSF9 expression between MSI and Non-MSI. Cox proportional hazards model and Kaplan–Meier curve were used for survival analysis. Spearman's correlation was used to investigate the association between TNFSF9 expression and immune cell infiltration. A significance level of $P<0.05$ was applied. Data visualization was performed using R software.

Results

MSI is associated with better survival

The experimental design is outlined in Fig. 1A. Survival analysis revealed that MSI was associated with better prognosis in STAD, as observed in the bulk RNA-seq data from GSE62254 ($P<0.05$; Fig. 1B). Cox regression

(See figure on next page.)

Fig. 5 Significance of cytokine-related pathways in MSI TME. **A** Volcano plot illustrating differential gene expression between MSI and Non-MSI. **B**–**D** GSEA, GO, and KEGG pathway enrichment analyses consistently identify the cytokine-cytokine receptor interaction pathway as significantly enriched in MSI. **E** RankNet analysis conducted with CellChat showing relative information flow of key signaling pathways between MSI and Non-MSI. **F** NetAnalysis SignalingRole heatmap conducted with CellChat uncovering distinct signaling patterns for MSI (left) and Non-MSI (right)

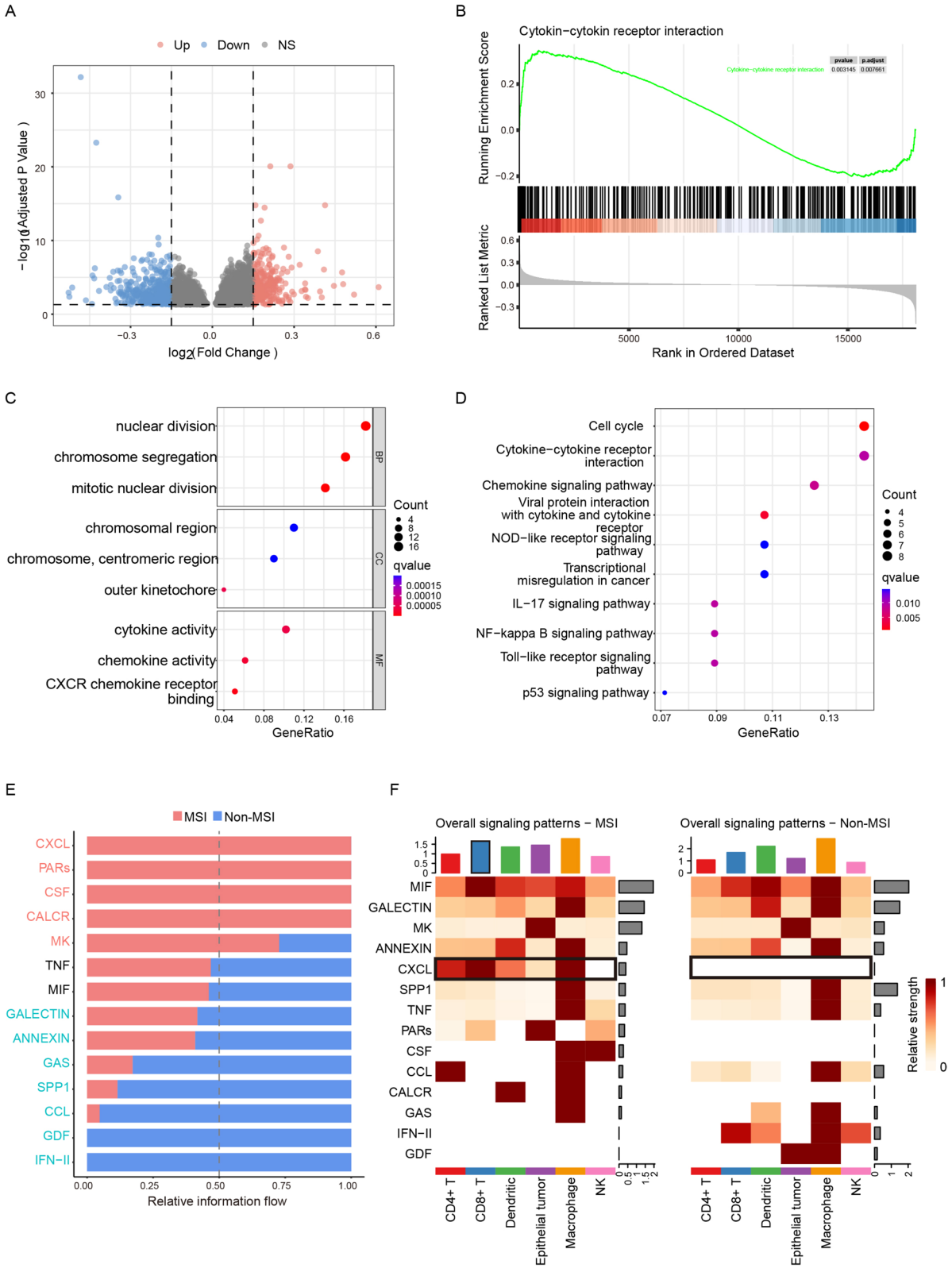

Fig. 5 (See legend on previous page.)

analysis of unadjusted covariates confirmed this association, which remained significant after adjusting for covariates (Table S1). These findings indicated that MSI is associated with better prognosis and survival.

TME heterogeneity between MSI and Non-MSI in bulk RNA-seq

We assessed the heterogeneity of TME between MSI and Non-MSI using bulk RNA-seq data (GSE62254). The analysis revealed no significant differences in immune score, stromal score or tumor purity score between MSI and Non-MSI ($P > 0.05$; Fig. 1C–E). To further characterize their immunologic landscape, we analyzed 22 immune infiltrating cells using the "CIBERSORT" algorithm. The results indicated that MSI exhibited a higher abundance of $CD4^+$ memory-activated T cells and M1 macrophages, but a lower abundance of $CD4^+$ memory-resting T cells, plasma cells, and eosinophils compared to Non-MSI (Fig. 1F).

TME heterogeneity between MSI and Non-MSI in scRNA-seq

We analyzed the single-cell-level heterogeneity of the TME between MSI and Non-MSI. Data quality control, PCA dimensionality reduction, and batch effect removal are shown in Fig. 2A–C. Based on cell lineage-specific marker genes (Figure S1A), the cells were classified into eight types: T&NK cells, B cells, epithelial cells, endothelial cells, fibroblasts, mast cells, myeloid cells, and plasma cells (Fig. 2D–E). The analysis revealed that T&NK cells constituted a higher proportion in MSI (46% vs. 34%), whereas plasma cells and fibroblasts were more abundant in Non-MSI (Fig. 2F).

We further analyzed lymphocytes within MSI (N = 7) and Non-MSI (N = 19). Distinct clusters of T&NK cells were identified by specific markers (Fig. 3A), including $CD4^+$T, $CD8^+$T, proliferating T cells (T pro) cells, and NK cells (Figure S1B). The results revealed an increased abundance of NK cells (14% *vs.* 11%) in MSI, while $CD4^+$T cells were more abundant in Non-MSI (Fig. 3B). No significant differences were observed in the proportions of T pro cells or $CD8^+$ T cells. Within the $CD8^+$ T cell population, distinct clusters were identified using marker genes (Figure S1C), including cytotoxic $CD8^+$T cells, effector memory $CD8^+$T cells, exhausted $CD8^+$T cells, mucosal-associated invariant T (MAIT) $CD8^+$ T cells, and naive $CD8^+$ T cells (Fig. 3C). The results indicated that exhausted $CD8^+$ T cells (23% vs. 13%) were more abundant in MSI, whereas effector memory $CD8^+$ T cells were more abundant in Non-MSI (Fig. 3D). Within the $CD4^+$T cell population, distinct clusters were identified using marker genes (Figure S1D), including naive $CD4^+$T cells, effector memory $CD4^+$T cells, regulatory $CD4^+$T cells, Th1-like $CD4^+$T cells, and Th17 $CD4^+$T cells (Fig. 3E). The analysis revealed that regulatory $CD4^+$ T cells (33% vs. 26%) and Th1-like $CD4^+$ T cells (15% vs. 11%) were enriched in MSI, whereas naive $CD4^+$ T cells and effector memory $CD4^+$ T cells were more abundant in Non-MSI (Fig. 3F).

Additionally, we conducted a subset analysis of myeloid cells within MSI and Non-MSI. Unique clusters of myeloid cells were identified using marker genes (Figure S1E), including monocytes, macrophages, and dendritic cells (DCs) (Fig. 4A). The analysis revealed that DCs (19% vs. 16%) and monocytes (53% vs. 34%) were more abundant in MSI, while macrophages were predominantly enriched in Non-MSI (Fig. 4B). Within the macrophage subtypes, distinct clusters were identified based on marker genes (Figure S1F), including M0 macrophages, M1 macrophages, and M2 macrophages (Fig. 4C). The results showed that M1 macrophages (40% vs. 28%) were more prevalent in MSI, whereas M0 and M2 macrophages were more abundant in Non-MSI (Fig. 4D). DCs were identified using marker genes (Figure S1G), including activated DCs, conventional dendritic cells 1 (cDC1s), conventional dendritic cells 2 (cDC2s), and plasmacytoid dendritic cells (pDCs) (Fig. 4E). Activated DCs (22% vs. 10%) and cDC1s (13% vs. 6%) were significantly enriched in MSI, whereas cDC2s were more abundant in Non-MSI (Fig. 4F).

Cytokine-related pathways in the TME of MSI

To further investigate the differences in the TME between MSI and Non-MSI, we initially screened for DEGs using bulk RNA-seq data. A total of 338 DEGs were identified, with selection criteria of fold change (FC) > 0.25

(See figure on next page.)

Fig. 6 TNFSF9 enhances antigen presentation and promotes anti-tumor responses in MSI. **A** Venn diagram depicting gene overlaps within cytokine-related pathways. **B**, **C** Boxplots showing increased TNFSF9 expression in MSI based on data from GSE62254 and TCGA databases. **D** FeaturePlot showing TNFSF9 expression across different STAD cell lines. **E** Violin plot illustrating heightened TNFSF9 expression in MSI tumor epithelial cells at the single-cell level. **F** IHC staining showed high TNFSF9 expression in MSI. a, IHC staining of TNFSF9 in MSI (magnification, × 200); b, IHC staining of TNFSF9 in MSI (magnification, × 200); c, IHC staining of TNFSF9 in Non-MSI (magnification, × 200); d, IHC staining of TNFSF9 in Non-MSI (magnification, × 400). **G** Mean IOD of TNFSF9 between MSI (N = 13) and Non-MSI (N = 10). **H** qPCR analysis comparing TNFSF9 expression between SNU-1 (MSI) and AGS (Non-MSI) cell lines. **I** WB analysis of TNFSF9 expression between SNU-1 (MSI) and AGS (Non-MSI) cell lines, with the original blot is in Supplementary Fig. 2. **J** Correlation analysis of TNFSF9 expression with M1 macrophages

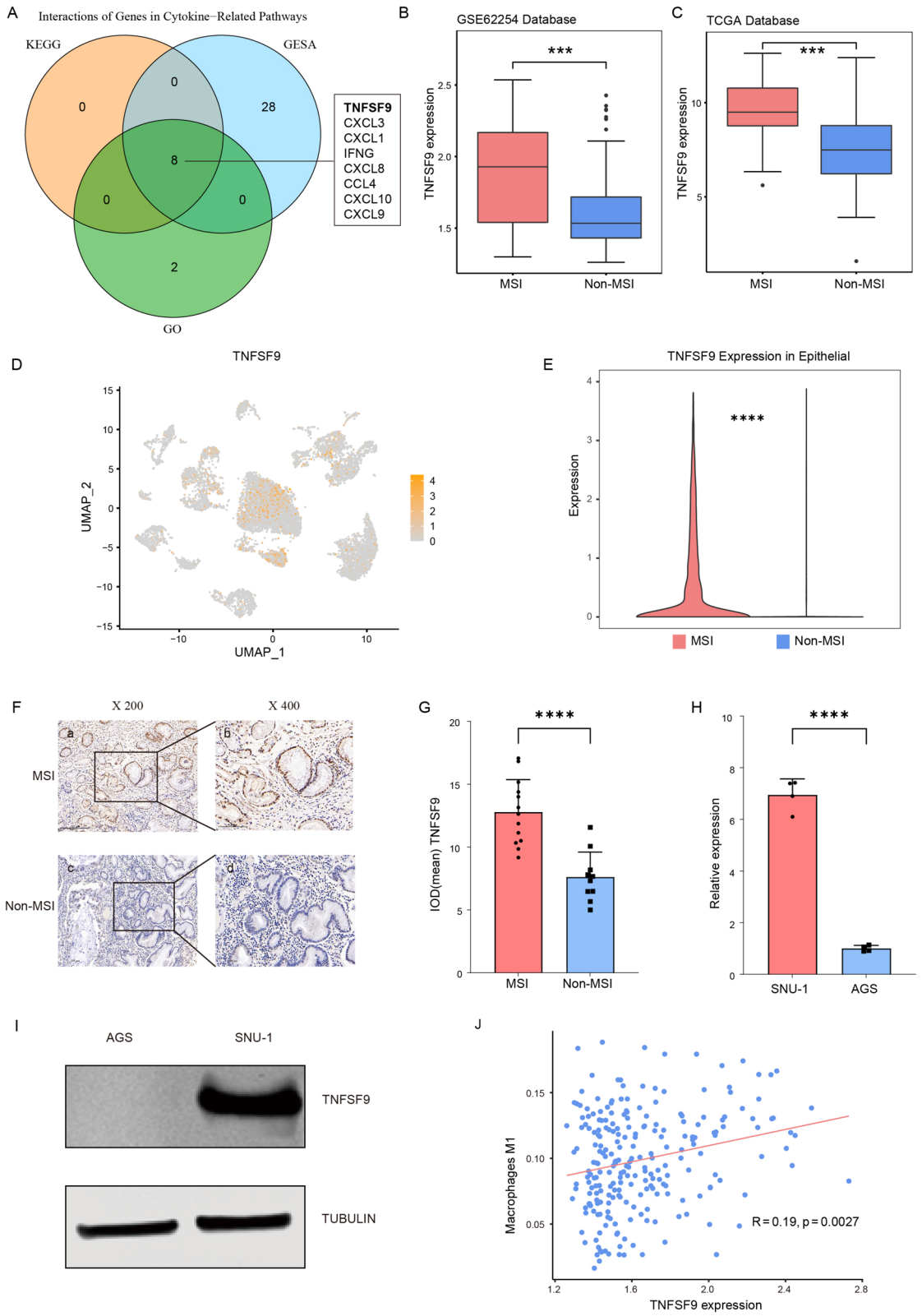

Fig. 6 (See legend on previous page.)

and adjusted $P < 0.05$. This set included 112 upregulated and 225 downregulated DEGs (Fig. 5A). GSEA analysis revealed significant enrichment of DEGs in the Cytokine-cytokine receptor interaction pathway (Fig. 5B). GO analysis highlighted the enrichment of DEGs in the Cytokine activity pathway (Fig. 5C). Similarly, KEGG analysis demonstrated a marked enrichment of DEGs in the Cytokine-cytokine receptor interaction pathway (Fig. 5D). Additionally, we performed cell-to-cell communication analysis using the "CellChat" package. The "RankNet" analysis revealed that the CXC chemokine ligand (CXCL) pathway exhibited significantly higher information flow in MSI (Fig. 5E). The "NetAnalysis Signaling Role heatmap" further confirmed the enrichment of CXCL in MSI (Fig. 5F).

TNFSF9 plays an important role in the TME of MSI

To identify key hub genes, we analyzed the overlap of genes associated with cytokine-related pathways and identified 8 hub genes (Fig. 6A). Notably, the expression of TNFSF9 was significantly higher in MSI across both GSE62254 and TCGA datasets (Fig. 6B, C). Subsequently, we conducted a single-cell analysis and observed that TNFSF9 was predominantly expressed in stromal cells, with partial expression in tumor epithelial cells in MSI (Fig. 6D, E). The expression of TNFSF9 in MSI and Non-MSI tissues was evaluated using IHC. The results showed that TNFSF9 expression was significantly higher in stromal cells and was also observed in tumor epithelial cells in MSI (Fig. 6F). Quantitative analysis of the IHC staining revealed that the mean IOD value of TNFSF9 was significantly higher in MSI (Fig. 6G). qPCR analysis showed higher TNFSF9 expression in the SNU-1 (MSI) cell line compared to the AGS (Non-MSI) cell line (Fig. 6H). Similarly, WB analysis confirmed higher TNFSF9 expression in SNU-1 (MSI) cells (Fig. 6I). To explore the relationship between TNFSF9 expression and immune infiltration, we examined its co-expression with 22 immune-related cell types. The analysis revealed a positive correlation with M1 macrophages, classified as antigen-presenting cells (APCs) (Fig. 6J).

Discussion

TCGA database classified STAD into four subtypes, including MSI, EBV, CIN and GS [1]. Recently, immune checkpoint inhibitors (ICIs) have demonstrated significant clinical efficacy in patients with MSI but limited efficacy in Non-MSI. Studies found that MSI was associated with a better prognosis, even without immunotherapy [7]. Consistent with these observations, our study confirmed that MSI was associated with better prognosis and survival. Previous studies highlighted the correlation between MSI and high tumor mutational burden, which promoted increased infiltration of $CD4^+$ T and $CD8^+$ T cells [11]. However, these studies did not clarify the detailed immune profile or the mechanisms underlying it. Thus, our approach integrated bulk RNA-seq and scRNA-seq analyses to provide a more comprehensive understanding of the TME differences between MSI and Non-MSI in STAD.

Notably, we observed a significant abundance of Th1-like $CD4^+$ T cells in MSI, which played a key role in antigen presentation. DCs enhanced antigen presentation with the help of $CD4^+$ T cells [27]. Th1 $CD4^+$ T cells induced type 1 immune responses by activating M1 macrophages to combat intracellular pathogens [28]. Following activation by APCs, Th1 $CD4^+$ T cells, differentiated from naive $CD4^+$ T cells, expressed CD40L and secreted cytokines such as IL-2, IFN-γ, and TNF to amplify their immune function [29]. Activated Th1 $CD4^+$ T cells played an essential role in immune responses by secreting IL-2 and other cytokines to stimulate cytotoxic T cell activation and support cellular immunity [30]. The interaction between APCs and Th1 $CD4^+$ T cells illustrated a mechanism that enhanced antigen presentation in MSI, promoting effective anti-tumor immunity.

However, we also observed instances of immunosuppression within MSI, primarily due to the increased abundance of regulatory T cells and "exhausted" $CD8^+$ T cells. Tregs were recognized for their role in suppressing tumor immunity; however, they also prevented autoimmunity by modulating excessive immune responses [27]. We verified that MSI exhibited robust immune responses and hypothesized that the overexpression of Tregs might have resulted from an exaggerated immune reaction. Additionally, a significant abundance of exhausted $CD8^+$ T cells was observed in MSI. Prolonged antigenic stimulation led to a dysfunctional state, termed "exhaustion," in tumor-specific $CD8^+$ T cells [31]. Despite the elevation of immunosuppressive cells in MSI, we proposed that sustained and potent antigenic stimulation, coupled with efficient antigen presentation, ultimately shifted the balance toward anti-tumor immunity. Moreover, studies showed that exhausted $CD8^+$ T cells regained their tumor-killing functionality upon treatment with ICIs [32]. This phenomenon partly explained the clinical benefits of immunotherapy in MSI tumors.

Furthermore, our analysis showed that MSI was associated with increased APCs. The connection between anti-tumor immunity and MSI cancers stemmed from MSI's tendency to accumulate frameshift mutations, making these cancers highly immunogenic [10]. The resulting neoantigens were linked to APCs activation, as indicated by the observed abundance of M1 macrophages and activated DCs in MSI. DCs, as professional APCs, played a crucial role in orchestrating adaptive immune responses

[33]. M1 macrophages, activated by T-helper type-1 cytokines, played a key role in inhibiting cell proliferation and inducing tissue damage [34]. The results highlighted that the abundance of tumor-associated antigens in MSI promoted activation of APCs and enhanced antitumor immunity.

In addition, further analysis of DEGs and pathway enrichment revealed a significant association between MSI and cytokine-related pathways. 8 hub genes were identified, with TNFSF9 standing out due to its exclusive expression in MSI, as observed in both bulk RNA-seq and scRNA-seq. TNFSF9, a member of the TNF superfamily, acted as a ligand for CD137 and was expressed in APCs [35, 36]. TNFSF9 was also expressed in various types of tumor cells [37, 38]. CD137, predominantly expressed in activated leukocytes, particularly T cells and DCs, played a critical role in immune activation [39]. Interaction with its ligand TNFSF9 activated key signaling pathways, including NF-κB, JNK/SAPK, and p38/MAPK, leading to the activation of $CD4^+$ and $CD8^+$ T cells [40]. Beyond T cells, this interaction bi-directionally activated APCs, such as monocytes, and facilitated the initiation of cytotoxic T-cell responses by activating DCs [41]. In summary, elevated TNFSF9 expression in MSI and its positive correlation with APCs suggest a critical role in shaping the MSI TME and enhancing immunotherapy effectiveness.

Finally, our integrative analysis of bulk RNA-seq and scRNA-seq data offered valuable insights into the immunological differences between MSI and Non-MSI. However, several limitations must be considered. While supported by existing literature, further in-depth mechanistic studies are needed to validate these findings and elucidate the underlying pathways.

While our study provides valuable insights into the immunological differences between MSI and Non-MSI in STAD through integrative bulk RNA-seq and scRNA-seq analysis, several limitations should be acknowledged. First, the findings are largely correlative, and further experimental validation is required to establish the causal mechanisms, particularly the role of TNFSF9 in epithelial cells and its impact on immune modulation. Second, the resolution of scRNA-seq analysis, while informative, may not fully capture rare cell populations or subtle transcriptional changes. Third, patient heterogeneity, such as clinical and demographic factors, was not accounted for and may influence the immune profiles observed. Finally, while TNFSF9 emerged as a hub gene, its mechanistic pathways in MSI require further exploration using functional studies. Addressing these limitations in future research will enhance the understanding of MSI-associated immune responses and their implications for immunotherapy.

Conclusions

In conclusion, this study highlighted significant differences in the TME of MSI and Non-MSI in STAD. MSI showed a higher abundance of antigen-presenting cells, including M1 macrophages and activated dendritic cells. Additionally, MSI was associated with pro-inflammatory Th1-like $CD4^+$ T cells and cytokine-related pathways. However, MSI also demonstrated elevated levels of regulatory $CD4^+$ T cells and exhausted $CD8^+$ T cells, indicating a complex immune landscape. TNFSF9 was identified as a potential hub gene upregulated in MSI, and its expression was positively correlated with M1 macrophages. These findings underscore the critical role of TNFSF9 in shaping the MSI-specific TME.

Supplementary Information

The online version contains supplementary material available at https://doi.org/10.1186/s40001-025-02471-0.

Supplementary Material 1: Supplementary Figure 1: Heatmaps showing the expression of genes specific to STAD cells,T&NK cells, $CD8^+$T cells, $CD4^+$T cells, Myeloid cells, Dendritic cells, and Macrophages.

Supplementary Material 2: Supplementary Figure 2: Original Western Blot Data. WB analysis of Tubulin expression between AGS and SNU-1 cell lines. WB analysis of TNFSF9 expression between AGS and SNU-1cell lines.

Supplementary Material 3: Supplementary Table 1: Univariate and multivariate Cox regression analysis.

Supplementary Material 4: Supplementary Table 2: Hub genes.

Acknowledgements

The authors would like to thank TCGA and GEO public datasets for gene expression and survival information collection.

Author contributions

Conceptualization: Jianlong Zhou, Yucheng Zhang, Yongfeng Liu; Methodology: Jianlong Zhou, Jiehui Li, Wenxing Zhang, Junjiang Wang, Xueqing Yao; Software: Jianlong Zhou; Investigation: Jianlong Zhou; Data curation: Jianlong Zhou; Writing—original draft preparation: Jianlong Zhou; Writing—review and editing: Jianlong Zhou; Visualization: Jianlong Zhou; Supervision: Yong Li; Project administration: Huolun Feng, Jiabin Zheng. Both authors have read and agreed to the published version of the manuscript.

Funding

Not applicable.

Availability of data and materials

No datasets were generated or analysed during the current study.

Declarations

Ethical approval and informed consent

The study was conducted in accordance with the Declaration of Helsinki and approved by the Institutional Review Board (or Ethics Committee) of the Ethics Committee of Guangdong Provincial People's Hospital, Ethical conduct of research Approved by the Ethics Committee of Guangdong Provincial People's Hospital (protocol code KY-Q-2021-263-01). Informed written consent was obtained from all participating patients, ensuring their voluntary participation and understanding of the study's objectives and procedures.

Consent for publication

Not applicable.

Competing interests
The authors declare no competing interests.

Author details
[1]Department of Gastrointestinal Surgery, Department of General Surgery, Guangdong Provincial People's Hospital (Guangdong Academy of Medical Sciences), Southern Medical University, Guangzhou 510080, Guangdong, China. [2]School of Medicine, South China University of Technology, Guangzhou 510006, Guangdong, China. [3]Department of General Surgery, Guangdong Provincial People's Hospital Ganzhou Hospital (Ganzhou Municipal Hospital), Ganzhou 341000, China.

Received: 21 May 2024 Accepted: 17 March 2025
Published online: 28 March 2025

References

1. Cancer Genome Atlas Research Network. Comprehensive molecular characterization of gastric adenocarcinoma. Nature. 2014;513(7517):202–9.
2. Baretti M, Le DT. DNA mismatch repair in cancer. Pharmacol Ther. 2018;189:45–62.
3. Zhang L. Immunohistochemistry versus microsatellite instability testing for screening colorectal cancer patients at risk for hereditary nonpolyposis colorectal cancer syndrome. Part II. The utility of microsatellite instability testing. J Mol Diagn. 2008;10(4):301–7.
4. Kang YK, Boku N, Satoh T, Ryu MH, Chao Y, Kato K, et al. Nivolumab in patients with advanced gastric or gastro-oesophageal junction cancer refractory to, or intolerant of, at least two previous chemotherapy regimens (ONO-4538-12, ATTRACTION-2): a randomised, double-blind, placebo-controlled, phase 3 trial. Lancet. 2017;390(10111):2461–71.
5. Janjigian YY, Shitara K, Moehler M, Garrido M, Salman P, Shen L, et al. First-line nivolumab plus chemotherapy versus chemotherapy alone for advanced gastric, gastro-oesophageal junction, and oesophageal adenocarcinoma (CheckMate 649): a randomised, open-label, phase 3 trial. Lancet. 2021;398(10294):27–40.
6. Ratti M, Lampis A, Hahne JC, Passalacqua R, Valeri N. Microsatellite instability in gastric cancer: molecular bases, clinical perspectives, and new treatment approaches. Cell Mol Life Sci. 2018;75(22):4151–62.
7. van Velzen MJM, Derks S, van Grieken NCT, Haj Mohammad N, van Laarhoven HWM. MSI as a predictive factor for treatment outcome of gastroesophageal adenocarcinoma. Cancer Treat Rev. 2020;86:102024.
8. Puliga E, Corso S, Pietrantonio F, Giordano S. Microsatellite instability in gastric cancer: between lights and shadows. Cancer Treat Rev. 2021;95:102175.
9. Rodriquenz MG, Roviello G, D'Angelo A, Lavacchi D, Roviello F, Polom K. MSI and EBV positive gastric cancer's subgroups and their link with novel immunotherapy. J Clin Med. 2020;9(5):1427.
10. Kloor M, von Knebel DM. The immune biology of microsatellite-unstable cancer. Trends Cancer. 2016;2(3):121–33.
11. Li B, Severson E, Pignon JC, Zhao H, Li T, Novak J, et al. Comprehensive analyses of tumor immunity: implications for cancer immunotherapy. Genome Biol. 2016;17(1):174.
12. De Rosa S, Sahnane N, Tibiletti MG, Magnoli F, Vanoli A, Sessa F, et al. EBV^{+} and MSI gastric cancers harbor high PD-L1/PD-1 expression and high CD8^{+} intratumoral lymphocytes. Cancers. 2018;10(4):102.
13. Kim JY, Kim WG, Kwon CH, Park DY. Differences in immune contextures among different molecular subtypes of gastric cancer and their prognostic impact. Gastric Cancer. 2019;22(6):1164–75.
14. Kim R, An M, Lee H, Mehta A, Heo YJ, Kim KM, et al. Early tumor-immune microenvironmental remodeling and response to first-line fluoropyrimidine and platinum chemotherapy in advanced gastric cancer. Cancer Discov. 2022;12(4):984–1001.
15. Zhang P, Yang M, Zhang Y, Xiao S, Lai X, Tan A, et al. Dissecting the single-cell transcriptome network underlying gastric premalignant lesions and early gastric cancer. Cell Rep. 2019;27(6):1934-47.e5.
16. Jiang H, Yu D, Yang P, Guo R, Kong M, Gao Y, et al. Revealing the transcriptional heterogeneity of organ-specific metastasis in human gastric cancer using single-cell RNA sequencing. Clin Transl Med. 2022;12(2): e730.
17. Kumar V, Ramnarayanan K, Sundar R, Padmanabhan N, Srivastava S, Koiwa M, et al. Single-cell atlas of lineage states, tumor microenvironment, and subtype-specific expression programs in gastric cancer. Cancer Discov. 2022;12(3):670–91.
18. Sathe A, Grimes SM, Lau BT, Chen J, Suarez C, Huang RJ, et al. Single-cell genomic characterization reveals the cellular reprogramming of the gastric tumor microenvironment. Clin Cancer Res. 2020;26(11):2640–53.
19. Newman AM, Liu CL, Green MR, Gentles AJ, Feng W, Xu Y, et al. Robust enumeration of cell subsets from tissue expression profiles. Nat Methods. 2015;12(5):453–7.
20. Stuart T, Butler A, Hoffman P, Hafemeister C, Papalexi E, Mauck WM 3rd, et al. Comprehensive integration of single-cell data. Cell. 2019;177(7):1888-902.e21.
21. Korsunsky I, Millard N, Fan J, Slowikowski K, Zhang F, Wei K, et al. Fast, sensitive and accurate integration of single-cell data with Harmony. Nat Methods. 2019;16(12):1289–96.
22. Jin S, Guerrero-Juarez CF, Zhang L, Chang I, Ramos R, Kuan CH, et al. Inference and analysis of cell-cell communication using Cell Chat. Nat Commun. 2021;12(1):1088.
23. Ritchie ME, Phipson B, Wu D, Hu Y, Law CW, Shi W, et al. limma powers differential expression analyses for RNA-sequencing and microarray studies. Nucleic Acids Res. 2015;43(7): e47.
24. Yu G, Wang LG, Han Y, He QY. clusterProfiler: an R package for comparing biological themes among gene clusters. OMICS. 2012;16(5):284–7.
25. Wang Z, Wang X, Xu Y, Li J, Zhang X, Peng Z, et al. Mutations of PI3K-AKT-mTOR pathway as predictors for immune cell infiltration and immunotherapy efficacy in dMMR/MSI-H gastric adenocarcinoma. BMC Med. 2022;20(1):133.
26. Li L, Yang M, Yu J, Cheng S, Ahmad M, Wu C, et al. A novel L-phenylalanine dipeptide inhibits the growth and metastasis of prostate cancer cells via targeting DUSP1 and TNFSF9. Int J Mol Sci. 2022;23(18):10916.
27. Borst J, Ahrends T, Bąbała N, Melief CJM, Kastenmüller W. CD4(+) T cell help in cancer immunology and immunotherapy. Nat Rev Immunol. 2018;18(10):635–47.
28. Zhu X, Zhu J. CD4 T helper cell subsets and related human immunological disorders. Int J Mol Sci. 2020;21(21):8011.
29. Romagnani S. Type 1 T helper and type 2 T helper cells: functions, regulation and role in protection and disease. Int J Clin Lab Res. 1991;21(2):152–8.
30. Kidd P. Th1/Th2 balance: the hypothesis, its limitations, and implications for health and disease. Altern Med Rev. 2003;8(3):223–46.
31. Dolina JS, Van Braeckel-Budimir N, Thomas GD, Salek-Ardakani S. CD8(+) T cell exhaustion in cancer. Front Immunol. 2021;12: 715234.
32. Jiang W, He Y, He W, Wu G, Zhou X, Sheng Q, et al. Exhausted CD8+T cells in the tumor immune microenvironment: new pathways to therapy. Front Immunol. 2020;11:622509.
33. Yin X, Chen S, Eisenbarth SC. Dendritic cell regulation of T helper cells. Annu Rev Immunol. 2021;39:759–90.
34 Boutilier AJ, Elsawa SF. Macrophage polarization states in the tumor microenvironment. Int J Mol Sci. 2021;22(13):6995.
35. Dharmadhikari B, Wu M, Abdullah NS, Rajendran S, Ishak ND, Nickles E, et al. CD137 and CD137L signals are main drivers of type 1, cell-mediated immune responses. Oncoimmunology. 2016;5(4): e1113367.
36. Harfuddin Z, Kwajah S, Chong Nyi Sim A, Macary PA, Schwarz H. CD137L-stimulated dendritic cells are more potent than conventional dendritic cells at eliciting cytotoxic T-cell responses. Oncoimmunology. 2013;2(11): e26859.
37. Qian Y, Pei D, Cheng T, Wu C, Pu X, Chen X, et al. CD137 ligand-mediated reverse signaling inhibits proliferation and induces apoptosis in non-small cell lung cancer. Med Oncol. 2015;32(3):44.
38. Dimberg J, Hugander A, Wågsäter D. Expression of CD137 and CD137 ligand in colorectal cancer patients. Oncol Rep. 2006;15(5):1197–200.
39. Sica G, Chen L. Biochemical and immunological characteristics of 4-1BB (CD137) receptor and ligand and potential applications in cancer therapy. Arch Immunol Ther Exp. 1999;47(5):275–9.

40. Geuijen C, Tacken P, Wang LC, Klooster R, van Loo PF, Zhou J, et al. A human CD137×PD-L1 bispecific antibody promotes anti-tumor immunity via context-dependent T cell costimulation and checkpoint blockade. Nat Commun. 2021;12(1):4445.
41. Langstein J, Michel J, Fritsche J, Kreutz M, Andreesen R, Schwarz H. CD137 (ILA/4-1BB), a member of the TNF receptor family, induces monocyte activation via bidirectional signaling. J Immunol. 1998;160(5):2488–94.

Publisher's Note